Irregular Pressure Induced Shift of the First UV-Absorption Band of 4-Nitroanisole in CO_2 and CHF_3

Guillermo A. Alvarez[a], Wolfram Baumann[a,b], Frank Neitzel[b], and Silvana V. Rodrigues[c]

[a] Departamento de Química, Facultad de Ciencias, Universidad de los Andes, Carrera 1 No. 18A-10/70, Bogotá, Colombia
[b] Institute of Physical Chemistry, University of Mainz, 55099 Mainz, Germany
[c] Departamento de Química Analítica, Instituto de Química, Universidade Federal Fluminense, 22.240-090 Niterói, RJ, Brasil

Reprint requests to Prof. G.A. A.; Fax: 005713324366; E-mail: gualvare@uniandes.edu.co

Z. Naturforsch. **64a,** 855 – 864 (2009); received January 20, 2009

The first UV-absorption band of the polar molecules trans-4-dimethylamino-4′-nitrostilbene (DMANS), 5-dimethylamino-5′-nitro-2,2′-bithiophene (DMANBT), and 4-nitroanisole (NA), and of the slightly polar pesticide diclofop-methyl in the nonpolar supercritical solvent carbon dioxide (CO_2) and in the slightly polar supercritical solvent trifluoromethane (CHF_3) was measured in the pressure range from 1.5 to 30 MPa and the temperature range from 298 to 353 K with the purpose of studying the solvent-solute interactions in these molecules. The theory of Liptay for the effect of the solvent on the wave number of the electronic absorption of the solute molecule was applied. In this theory the solvent is represented by an isotropic and homogeneous dielectric continuum characterized by a pressure and temperature dependent dielectric constant $\varepsilon(P,T)$, and an optical refraction index n. For the isotherms which approach the critical point in both solvents there is a change in the slope of the plot of the wave number maximum against the solvent parameter $g = (\varepsilon - 1)/(2\varepsilon + 1)$ which is reminiscent of complex formation. A possible mechanism for this phenomenon is the arrangement of the solvent molecules around the dilute solute in the intermediate region at the (continuous) transition of the solvent from the dense vapour to the supercritical fluid.

Key words: Dielectric Interactions; Dispersion; Pressure Dependent UV-Absorption; Supercritical CO_2; Supercritical CHF_3; Complex Formation.

1. Introduction

The description of macroscopic equilibrium and non-equilibrium processes in gases and liquids needs first of all good understanding of the intermolecular interactions between the given molecules on a microscopic scale [1, 2], but finally models are to be built that relate molecular properties to observable (bulk) properties of the considered macroscopic system. In many cases relatively simple models yield good descriptions but in others the simple models may fail. Modelling e. g. the solvent polarity induced shift of absorption spectra of solute molecules by simple functions of the dielectric constant ε, and the optical refractive index n, usually yields large scatter around the ideal relation. Many authors have studied this solvent shift effect [3 – 7] and Liptay's [3] detailed model may be considered the most elaborate one – see also [8] for further details. In this model effects are attributed to polarization and dispersion interactions between the dissolved molecule and the surrounding solvent molecules. Both classical and quantum mechanical calculations agree while the latter deals additionally with the dispersion interactions. Practical experiments are limited by the available solvent polarities, in particular at the low polarity side below $\varepsilon \approx 2$. Thus solvent shift experiments in the range $1 < \varepsilon < 2$ are highly desirable. This can be done using sub- and supercritical fluids where ε can easily be varied by pressure and/or temperature. An additional advantage then is that specific interactions between the solute and the solvent responsible for the experimental scatter are not changed, as they would be with changing the solvent. The range $\varepsilon < 2$ is in particular interesting when passing through the critical point since one then might hope to get new knowledge on how a molecule passes from its isolated (gas phase) state to the dense environment in a liquid or pseudo-liquid state, building up a nearby fluid or solvent environment. In order to study this low polarity range NA has been studied in CO_2 and

0932–0784 / 09 / 1200–0855 $ 06.00

CHF_3 down to as low densities as only limited by its solubility.

2. The Basic Model [3, 9]

A free molecule (superscript $^\circ$) in its electronic ground state g has the energy $E_g{}^\circ$, a permanent electric dipole moment $\mu_g{}^\circ$, and polarizability $\alpha_g{}^\circ$. (α is a second-order symmetric tensor, μ is a column vector, and $\mu^\dagger$ is its row vector, $\mu^\dagger\mu$ is a scalar, and $\mu\mu$ is a second-order tensor). The solvent is considered as an isotropic and homogeneous dielectric continuum with a dielectric constant ε, and an optical refractive index n.

The molecule in the ground state g is now brought into an empty cavity prepared in the solvent. The solution is sufficiently dilute so that there are no interactions among the solute molecules. The process of making the cavity in the solvent requires an energy E_{Cg}, and by placing the molecule in this cavity the system is stabilized by dispersion interactions by an amount E_{Dg} and by the interactions of the dipole $\mu_g{}^\circ$ of the solute molecule with the surrounding dielectric by an amount W_g.

The total (permanent plus induced) dipole moment μ_g of the dissolved molecule is (in the absence of an external electric field):

$$\mu_g = \mu_g{}^\circ + \alpha_g{}^\circ E_{Rg}. \tag{1}$$

$\alpha_g{}^\circ$ is the ground state polarizability tensor of the solute. E_{Rg} is called the Onsager reaction field. In spherical approximation it is

$$E_{Rg} = f\mu_g, \tag{2}$$

where f is given by

$$f = \frac{1}{4\pi\varepsilon_0}\frac{2}{a^3}\frac{\varepsilon-1}{2\varepsilon+1}; \tag{3}$$

ε_0 is the permittivity of vacuum ($\varepsilon_0 = 8.854\times10^{-12}$ $C^2\,N^{-1}\,m^{-2}$) and a^3 is the third power of the so-called Onsager radius, proportional to the solute's interaction volume. Note that f includes orientation as well as electronic polarization.

For future use the quantity g is defined as

$$\frac{\varepsilon-1}{2\varepsilon+1} = g. \tag{4}$$

Putting (2) into (1) yields the relation between the in solution effective dipole moment μ_g and $\mu_g{}^\circ$:

$$\mu_g = (\mathbf{1} - f\alpha_g{}^\circ)^{-1}\mu_g{}^\circ. \tag{5}$$

For the Franck-Condon (FC) excited state the considerations are similar and

$$\mu_a = \mu_a{}^\circ + \alpha_a{}^\circ E_{Ra}, \tag{6}$$

except that the orientation polarization is due that of the ground state. $\mu_a{}^\circ$ is the FC excited state dipole moment and $\alpha_a{}^\circ$ its polarizability tensor. Therefore,

$$E_{Ra} = (f - f')\mu_g + f'\mu_a. \tag{7}$$

The positive quantity f' is defined similarly to (3) and takes into account the electronic polarization only:

$$f' = \frac{1}{4\pi\varepsilon_0}\frac{2}{a^3}\frac{n^2-1}{2n^2+1}. \tag{8}$$

n is the refractive index of the solvent extrapolated to wave number $\tilde\nu = 0$.

The definition of a μ_a similar to μ_g in (5) then yields a more complicated expression:

$$\begin{aligned}\mu_a = {} & (\mathbf{1} - f'\alpha_a{}^\circ)^{-1}\mu_a{}^\circ \\ & + (f - f')\alpha_a{}^\circ(\mathbf{1} - f'\alpha_a{}^\circ)(\mathbf{1} - f\alpha_g{}^\circ)^{-1}\mu_g{}^\circ.\end{aligned} \tag{9}$$

Note that in nonpolar solvents the second term vanishes.

The interaction of these total dipole moments (5) and (9) with the respective reaction fields then yields an energy lowering, different in the ground and the excited state, and therefore to a red or blue shift of the respective absorption or fluorescence band. The detailed further description by Liptay then relates the absorption wavenumber in solution $\tilde\nu_a{}^{Soln}$ to the value for the free molecule $\tilde\nu_a{}^\circ$ and the dielectric properties of the solvent:

$$\begin{aligned}hc\tilde\nu_a{}^{Soln} = {} & hc\tilde\nu_a{}^\circ - hcDf' \\ & - f'(\mu_a{}^{\circ\dagger} - \mu_g{}^{\circ\dagger})(\mathbf{1} - f'\alpha_a{}^\circ)^{-1}(\mu_a{}^\circ - \mu_g{}^\circ)/2 \\ & - f(\mu_a{}^{\circ\dagger} - \mu_g{}^{\circ\dagger})(\mathbf{1} - f\alpha_g{}^\circ)^{-1}\mu_g{}^\circ \\ & - f\mu_g{}^{\circ\dagger}(\mathbf{1} - f'\alpha_a{}^\circ)^{-1}(1 - f\alpha_g{}^\circ)^{-2}(\alpha_a{}^\circ - \alpha_g{}^\circ) \\ & \cdot [f(1 - f'\alpha_g{}^\circ)\mu_g{}^\circ/2 + f'(1 - f\alpha_g)(\mu_a{}^\circ - \mu_g{}^\circ)].\end{aligned} \tag{10}$$

D in this equation is the difference of the dispersion energies of the solute in the excited and the ground state.

Solute solvent complexes are assumed to be negligible in this description.

Usually, the last term in (10) is neglected as being small compared to the other dipole moment governed terms. Furthermore, if f' does not differ much from f the simpler relationship

$$\begin{aligned} &hc\tilde{\nu}_a^{\,\mathrm{Soln}} = \text{const.} \\ &-f(\mu_a{}^{\circ\dagger} - \mu_g{}^{\circ\dagger})(\mathbf{1} - f\alpha_a{}^{\circ})^{-1}(\mu_a{}^{\circ} - \mu_g{}^{\circ})/2 \\ &-f(\mu_a{}^{\circ\dagger} - \mu_g{}^{\circ\dagger})(\mathbf{1} - f\alpha_g{}^{\circ})^{-1}\mu_g{}^{\circ} \\ &\approx \text{const.} - f(\mu_a{}^{\circ\dagger} - \mu_g{}^{\circ\dagger})(\mathbf{1} - f\alpha_g{}^{\circ})^{-1}\mu_g{}^{\circ} \end{aligned} \tag{11}$$

or the simplest version for rigid molecules

$$hc\tilde{\nu}_a^{\,\mathrm{Soln}} = \text{const.} - f(\mu_a{}^{\circ\dagger} - \mu_g{}^{\circ\dagger})\mu_g{}^{\circ} \tag{12}$$

may be used to estimate for example $\mu_a{}^{\circ}$ from the slope of the respective plot, if $\mu_g{}^{\circ}$ is known.

The same basic ideas used here have recently been applied to model the solubility of organic molecules in supercritical CO_2 and CHF_3 [10] and the chromatographic retention times of pesticides in supercritical CO_2 [11].

3. Experimental Results

3.1. Experimental

The absorption spectra of the model compounds in pressurized CO_2 and CHF_3 were measured in a temperature controlled stainless steel cell described elsewhere [12], directly attached to a Perkin Elmer Lambda 15 spectrophotometer, run under UV WINLAB on a standard personal computer.

Pressure dependent g-values according to (4) were calculated using the pressure dependence of ε measured for CO_2 by [13] and for CHF_3 by [14].

3.2. Model Systems

In order to study the absorption behaviour of polar compounds in the low polarity range $\varepsilon < 2$ NA was selected due to its relatively good solubility in CO_2. In addition some helpful information from previous measurements was available. Its ground and excited state dipole moments have been measured by electrooptical absorption experiments and it was shown that they are parallel in good approximation [15], and its solvatochromic shift has been studied before [9, 16]. Due to its sufficiently large dipole moments it was also assumed that dispersion and explicit polarizability terms might be neglected (see below). It is to be mentioned here too that the absorption band of NA in CO_2 under all studied conditions is broad and unstructured and does not show any ε or pressure dependent change of its form.

4. Results

4.1. Solvatochromic Shifts of Nonpolar Molecules in Supercritical CO_2

The dispersion contribution can be estimated for nonpolar molecules where $\mu_g{}^{\circ} \approx \mu_a{}^{\circ} \approx 0$. It is easily shown that this contribution is negligible for polar molecules. Neglecting polarizability terms, assuming that the ground and excited state dipole moments are parallel and for nonpolar solvents in which the Maxwell relation $\varepsilon = n^2$, is assumed to be valid, (10) simplifies to

$$\tilde{\nu}_a^{\mathrm{Soln}} = \tilde{\nu}_a{}^{\circ} - \frac{1}{4\pi\varepsilon_0}\frac{1}{a^3 hc}[(\mu_a{}^{\circ})^2 - (\mu_g{}^{\circ})^2 + 2hcD]g. \tag{13}$$

The quantum mechanical calculations of Liptay [3] show that D is a positive quantity (red shift) which is to a first approximation independent of the solvent and which consists of two terms. The first term contains only energy levels of the dissolved molecule and the second term depends additionally on the transition

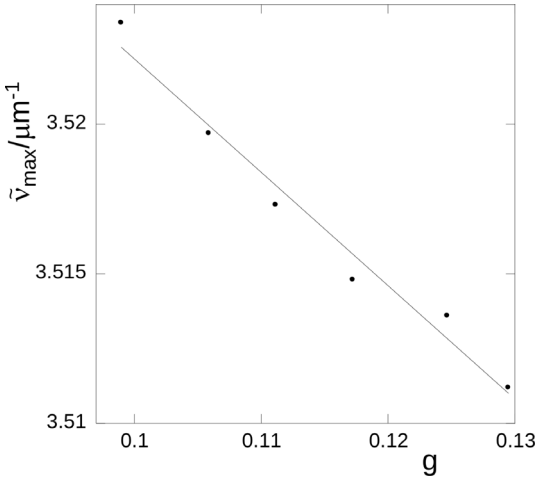

Fig. 1. Wave number of the maximum of the absorption of the nonpolar pesticide diclofop-methyl in supercritical CO_2 at 313 K against the quantity $(\varepsilon - 1)/(2\varepsilon + 1) = g$. The solid line is the regression line.

probability of the band under consideration. This implies that the red shift increases with increasing intensity of the absorption but also that a shift is present no matter how weak the absorption band may be.

The solvatochromic shift measurements on the pesticide diclofop-methyl in supercritical CO_2 at 313 K as a function of the parameter g are given in Figure 1. The measurements give a good straight line with a regression coefficient $r = 0.987$ despite the very small shifts near the limit of the resolution of the spectrophotometer.

In so far as all molecules are supposed to show dispersion interactions, the theory of Liptay [3] predicts a red shift contribution due to dispersion for all dissolved molecules. However, Neitzel [9] reports no discernible solvatochromic shift for the nonpolar pesticides isoproturon, dichlorprop, diuron, and dienochlor.

4.2. Solvatochromic Shifts of the Polar Molecules in Supercritical CO_2 and CHF_3

For the discussion below it is useful to consider briefly the phase diagrams of CO_2 and CHF_3. A projection of the equilibrium liquid-vapour surface for CO_2 onto the P-g plane [13] is shown in Figure 2. The g coordinate takes the place of the density ρ. (The relationship g-ρ is slightly nonlinear.) This plot includes the liquid-vapour coexistence line which encloses the two-phase liquid-vapour region and which terminates at the critical point ($T_C = 304.1$ K, $g_C = 0.07555$ marked by an X). With the temperature axis perpendicular to the plane of the paper and the critical point on the plane of the paper, the subcritical liquid CO_2 isotherm at 298 K lies on a plane above the plane of the paper (298 K $< T_C$) and terminates on the liquid-vapour coexistence line at the vapour pressure of CO_2 ($P_{vap} = 6.433$ MPa at 298 K). The supercritical CO_2 isotherms at 313 K to 353 K (313 K $> T_C$) on the other hand lie on planes behind the critical plane of the paper and since the liquid-vapour coexistence region ends at the critical point, the supercritical isotherms never meet this region as the pressure is lowered. That is all the supercritical isotherms transform continuously into a subcritical dense gas. The isotherms, shown by solid lines on this plot, correspond to the range of the measurements to be discussed below and the meaning of the dashed lines is also given below.

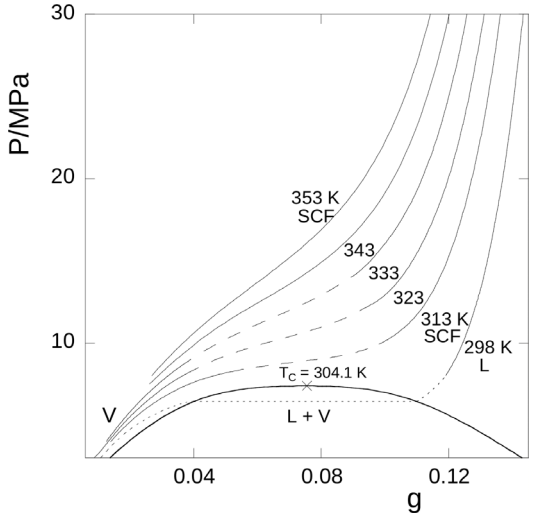

Fig. 2. Projection of the liquid-vapour equilibrium surface for CO_2 onto the P-g plane showing the region (L + V) enclosed by the liquid-vapour coexistence curve, the critical point (X) at $T_C = 304.1$ K, the subcritical liquid (L) isotherm at 298 K, and the supercritical (SCF) isotherms at 313 K, 323 K, 333 K, 343 K, and 353 K. Each isotherm is drawn corresponding to the range of the absorption measurements in this work. For the meaning of the dashed lines (---) in each isotherm see the text. The dotted line (· · ·) from the end of the 298 K liquid isotherm to the liquid-vapour coexistence line and through to the vapour region (V) does not represent measurements in this range.

Away from the Critical Point

The measurements at the subcritical liquid CO_2 temperature of 298 K and for the supercritical isotherms at 343 K and 353 K, which are far away from the critical point are particularly simple to analyze according

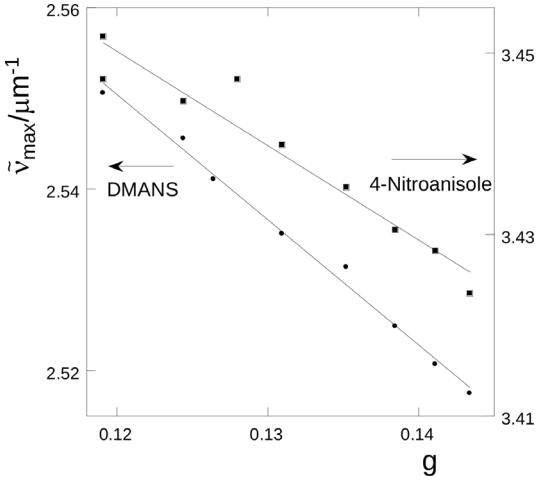

Fig. 3. Wave number of the maximum of the absorption of the polar molecules DMANS (•, left vertical scale) and NA (■, right vertical scale) in subcritical liquid CO_2 at 298 K against the parameter g. The solid lines are the regression lines.

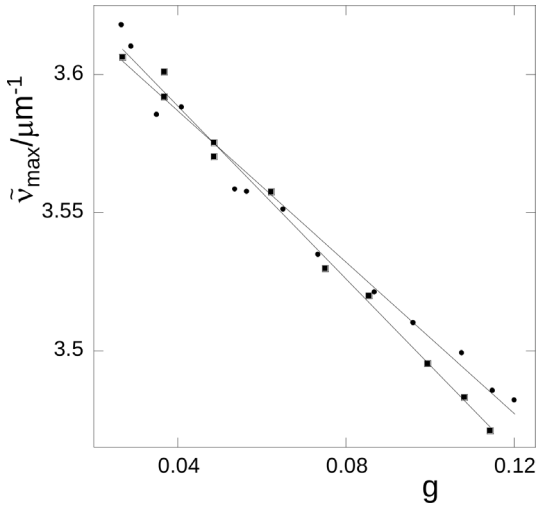

Fig. 4. Wave number of the maximum of the absorption of NA in supercritical CO_2 at 343 K (●) and 353 K (■) against g. The solid lines are the regression lines.

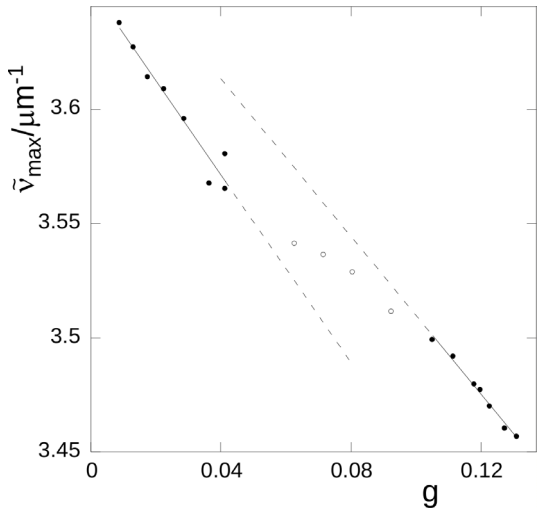

Fig. 5. Wave number of the maximum of the absorption of NA in supercritical CO_2 at 323 K against g. The solid lines are the regression lines through the solid symbols (●) and the dashed lines are the extrapolations of the regression lines. For the meaning of the hollow symbols (○) in the intermediate region see the text.

to Liptay's theory. Note that these isotherms are represented in Figure 2 by continuous solid lines. (The dotted line extending from the 298 K liquid isotherm to the first-order liquid-vapour phase transition and ending in the vapour does not represent any measurements in this region.)

Figure 3 shows the wave number of the maximum of the absorption of the polar molecules DMANS and NA in subcritical liquid CO_2 at 298 K against the parameter g. In agreement with (13), good straight lines are observed in this plot. The slope of the line is influenced by the quantities $\mu_g{}^\circ$, $\mu_a{}^\circ$, D, and a^3.

Similarly, the wave number of the maximum of the absorption of NA in supercritical CO_2 at 343 K and 353 K is plotted in Figure 4 against g. The regression line at 353 K has a correlation coefficient $r = 0.997$.

Near the Critical Point

A different behaviour of the plot of the wave number of the maximum of the absorption against g is obtained for the supercritical CO_2 and supercritical CHF_3 (and supercritical N_2O from the literature, see below) isotherms at 313 K, 318 K, 323 K, and 333 K which lie nearer to the critical point. A typical plot is shown in Figure 5 for NA in supercritical CO_2 at 323 K. It was pointed out by Neitzel [9] that these plots consisted of three regions namely an initial region at low g and a final region at high g separated by an intermediate region. The data in the low and in the high g regions both appear to obey Liptay's prediction, i. e. a linear relation between the wave number maximum and g. In Figure 5, for example, the regression coefficients of the low and the high regions are $r = 0.971$ and $r = 0.995$, respectively. The measurements in the intermediate region connect smoothly the high and low regions by an S-shaped curve. This intermediate region corresponds to the dashed lines in the isotherms in Figure 2 and is roughly the region of the continuous transition from the subcritical vapour to the supercritical fluid state. The isotherms at 343 K and 353 K in Figure 2 on the other hand where the intermediate region does not appear in the data (see Figure 4) are characterized by almost no change of slope at the transition between the two regions.

Measurements in Supercritical CHF_3

The projection of the equilibrium liquid-vapour surface for CHF_3 [14] is presented in Figure 6 analogous to Figure 2. Again the supercritical isotherms at 313 K and 323 K are drawn to correspond to the range of the measurements presented below and the dashed line in the 323 K isotherm represents the measurements in the intermediate region which appears by taking into account the low and high g regions (see Fig. 8 below). Compared to CO_2 the width of the intermediate region indicated by the dashed line on the 323 K

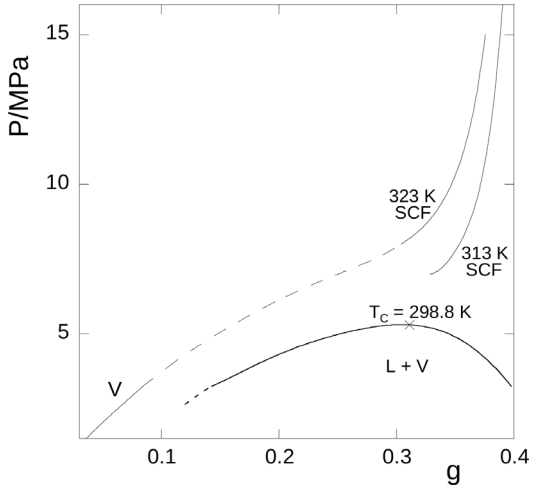

Fig. 6. Projection of the liquid-vapour equilibrium surface for CHF_3 onto the *P*-*g* plane showing the region (L + V) below the liquid-vapour coexistence curve, the critical point (X) at $T_C = 298.8$ K, the vapour region (V) and two supercritical (SCF) isotherms at 313 K and 323 K. Each isotherm is drawn corresponding to the range of the absorption measurements in this work. The dashed lines correspond to the intermediate region identified in applying Liptay's theory.

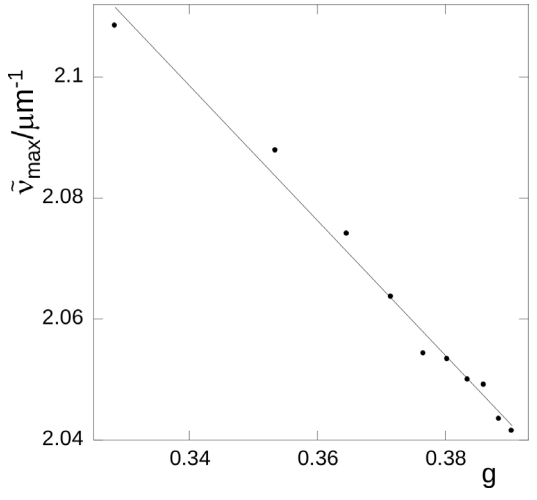

Fig. 7. Wave number of the maximum of the absorption of DMANBT in supercritical CHF_3 at 313 K against *g*. The solid line is the regression line.

isotherm for CHF_3 extends over a much wider range of *g* values.

Figure 7 presents the wave number maximum of DMANBT in supercritical CHF_3 at 313 K against *g*. The data in this figure correspond to the high *g* region (see Figure 6) and hence a smooth straight line is fitted through the points.

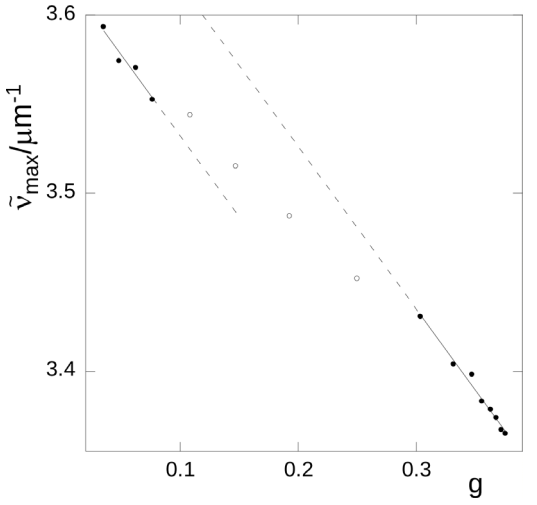

Fig. 8. Wave number of the maximum of the absorption of NA (filled circles (•) low and high *g* regions, hollow circles (○) intermediate region) in supercritical CHF_3 at 323 K against *g*. The solid lines are the regression lines through the filled symbols in the low and the high *g* regions and the dashed lines are the extrapolations of the regression lines.

Figure 8 shows the wave number maximum against *g* of NA in supercritical CHF_3 at 323 K. Similarly to the case described in Figure 5 the measurements on this isotherm are separated into low, intermediate, and high *g* regions.

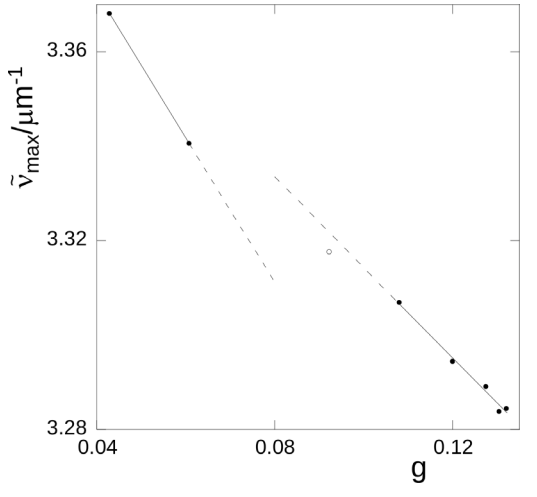

Fig. 9. Wave number of the maximum of the absorption of 2-nitroanisole (filled circles (•) low and high *g* regions, hollow circles (○) intermediate region) in supercritical nitrous oxide (N_2O) at 323 K against *g* from the data of Yonker et al. [17]. The solid lines are the regression lines through the filled symbols in the low and the high *g* regions and the dashed lines are the extrapolations of the regression lines.

Other Measurements

The data of Yonker et al. [17] for the wave number of the maximum of the absorption of 2-nitroanisole in supercritical nitrous oxide (N_2O) at 323 K are plotted against g in Figure 9 using the equilibrium liquid-vapour data for supercritical N_2O of Moriyoshi et al. [13]. Despite the few points the low and the high g regions and the intermediate region are recognized from the data. Due to the similarity of the N_2O molecule with CO_2 the extent of these regions in the g scale are practically coincident.

Similar data were also reported by Kajimoto et al. [18] for (N,N-dimethylamino)benzonitrile in supercritical CHF_3 at 323 K. These authors analyzed two different UV-absorption bands of the molecule. The different g regions coincide with the corresponding regions in Figure 8.

5. Discussion

Several authors [9, 17 – 21] have investigated solvent-solute interactions using supercritical fluids to alter in the first instance the density of the fluid and thus modify the amount of interaction. The effect of the pressure on the wave number of the absorption [9, 17, 18], on chemical equilibria [19, 21], and on the state of solvation of the solute in the supercritical fluid [20] have been studied. The theory of Liptay [3] or similar theories [5] based on Onsager's reaction field theory have been used by most of these authors [9, 17, 18, 21]. All of the authors encountered a deviation from an expected "normal" behaviour as the density was decreased from the dense fluid. Only two of the authors [9, 19] report measurements which cover the complete range from the gaseous state to the high density supercritical fluid. Kimura and Yoshimura [19] analyze the density dependence of the equilibrium constant of the dimerization equilibrium of 2-methyl-2-nitrosopropane in CO_2 and CHF_3 by dividing the density region into "three characteristic regions: low- and high-density regions, and a medium-density region". The authors attribute the deviations in the intermediate region to the large density fluctuations which appear through multibody interactions near the critical point. Kajimoto et al. [18] propose a mechanism for the change of the solvation number or clustering with increasing density of the fluid medium. Enhanced local density of the solvent around the solute relative to the bulk liquid strengthens the dielectric interaction between the fluid and the solute molecule thus increasing the shift of the absorption away from the gas phase for a given value of g. Computer simulations [22] and integral equation theories [23] have been used to elucidate the microscopic problem.

The phase diagrams of Figures 2 and 6 clearly show the almost abrupt change of slope of the isotherms between 313 K and 333 K once from the vapour to the intermediate, dashed line region and again from the intermediate to the supercritical fluid, solid line region. The isotherms at and above 343 K where the phenomenon of the intermediate g region does not appear in the data are characterized by almost no such change in the slope. The similarity of the continuous vapour to supercritical fluid transition with the discontinuous first-order vapour to liquid transition where an actual break in the slope takes place as illustrated by the 298 K isotherm in Figure 2 may be an indication for the appearance of the intermediate g region. (If an actual first-order transition were occurring in the supercritical fluid there would be two phases of constant density present and no change in the solvent power and hence no solvatochromic shift for the whole of the transition; this would explain the break in the slope in the intermediate region but there can be no first-order transition in the supercritical fluid.)

Mechanisms for continuous phase transitions are known in alloys and in liquid helium around 2 K among others [24]. An equimolecular alloy of copper and gold in the neighbourhood of the Curie temperature ($T_C \sim 710$ K) exhibits anomalies in the heat capacity and the coefficient of thermal expansion but not in the volume. At low temperatures each copper atom in the crystal structure is surrounded by gold atoms as nearest neighbours and vice versa, in a perfect long range order. As the temperature is raised, the gold atoms begin to exchange places with the copper atoms with a lowering of the long range order and at the Curie point the long distance order has disappeared completely. The difference between the two extreme cases of perfect order and perfect disorder arises because in the perfect order case the exchange of a gold atom with a copper atom requires a profound alteration of the surroundings of each atom and hence an expenditure of energy whereas in the atoms at random all sites are, on the average, equivalent and no energy is required for the exchange process. The explanation of these cooperative phenomena in which the energy needed for a process depends on the state of the whole system is clearly a major undertaking. In the present system

the high g region would correspond to the perfectly ordered lattice or its liquid phase equivalent while the gas phase or low g region would be totally random. In the transition region activation processes would provide sufficient energy in the form of thermal fluctuations to remove the solute molecule from its site, simultaneously accommodate a solvent molecule in its place, and set in motion the solute molecule to another suitable location.

It is possible to assume a solvation mechanism based on the theory of complex formation in solution [25] to attempt to elucidate the appearance of the intermediate region in the data. The results are presented below. A similar model was formulated by Kajimoto et al. [18] using statistical mechanics.

6. The Solvation Model [25]

The consecutive equilibria of a "step" system composed of a central group M (the solute) and up to N ligands A that surround it

$$\begin{aligned} &M + A \rightleftarrows MA, \\ &MA + A \rightleftarrows MA_2, \\ &\vdots \\ &MA_{N-1} + A \rightleftarrows MA_N \end{aligned} \tag{14}$$

are known to apply to acid-base equilibria, redox systems, and inorganic and organic complex formation.

The equilibrium constants valid for small concentrations of the reacting substances are given by

$$K_1 = \frac{[MA]}{[M][A]},\ K_2 = \frac{[MA_2]}{[MA][A]},\ \cdots,\ K_N = \frac{[MA_N]}{[MA_{N-1}][A]}. \tag{15}$$

The square brackets denote concentrations of the individual species but more generally activities must be employed in place of concentrations.

The usual task is to determine the concentration constants of the system from knowledge of $\tilde{n}$, the average number of ligands attached to M,

$$\tilde{n} = \frac{[MA] + 2[MA_2] + \cdots + N[MA_N]}{[M] + [MA] + [MA_2] + \cdots + [MA_N]}, \tag{16}$$

as a function of the free ligand concentration $[A]$; this is achieved by inserting the expressions (15) for the formation constants of the system in (16) with the result

$$\tilde{n} = \frac{\sum_{n=1}^{N} n\beta_n [A]^n}{1 + \sum_{n=1}^{N} \beta_n [A]^n}, \tag{17}$$

where β_n represents the product of constants $K_1 K_2 \ldots K_n$.

It is now assumed that the ratio between consecutive constants is at least to some extent statistically determined. Thus, if the tendency of compound MA_n to liberate one ligand is proportional to n, and its tendency to add a ligand is proportional to $N-n$, the N consecutive constants are then proportional to the quantities $N/1,\ (N-1)/2,\ \ldots,\ (N-n+1)/n,\ \ldots,\ 2/(N-1),\ 1/N$, provided other effects such as asymmetry (coordinative positions of different kind), and chemical and electrical forces are not present.

In the literature of the step equilibria (14) in general [25], it is customary to express the constants in terms of an average constant K and a spreading factor x, a constant quantity for the whole system, which takes values between 0 and ∞ and is based on achieving the greatest possible symmetry; then all the constants of the system are given by

$$K_n = \frac{N-n+1}{n} K x^{N+1-2n}. \tag{18}$$

The value $x = 1$ corresponds to the purely statistical case considered above. Upon introducing (18) into (17) a simple expression is obtained:

$$\tilde{n} = \frac{\sum_{n=1}^{N} n\binom{N}{n} K^n [A]^n x^{n(N-n)}}{1 + \sum_{n=1}^{N} \binom{N}{n} K^n [A]^n x^{n(N-n)}}, \tag{19}$$

where the symbol $\binom{N}{n}$ represents the binomial coefficient $\frac{N!}{(N-n)!n!}$. It is characteristic of (19) that at the midpoint of the curve ($\tilde{n}/N = 0.5$) (19) is satisfied by $K[A] = 1$, hence K is determined from $[A]_{\tilde{n}/N=0.5}$.

From the midpoint of the curve and the extrapolated zero solvatochromic shift the solvatochromic shift scale is converted to degree of formation $\tilde{n}/N$. Furthermore, due to the low solubility of the substances the free ligand concentration $[A]$ is approximated by the density of the fluid. Finally, slightly better results are obtained if instead of the density of the fluid the very similar quantity g is used as the activity. (Formally, the similarity of the density with g stems from the expansion of which the first term is known as the Clausius-Mossoti equation $(\varepsilon - 1)/(\varepsilon + 2) = A\rho$, where ρ is the density and A is a constant. Cf. $g = (\varepsilon - 1)/(2\varepsilon + 1)$.)

The data of Figure 5 for the wave number of the maximum of the absorption of NA converted to degree of complex formation $\tilde{n}/N$ in supercritical CO_2

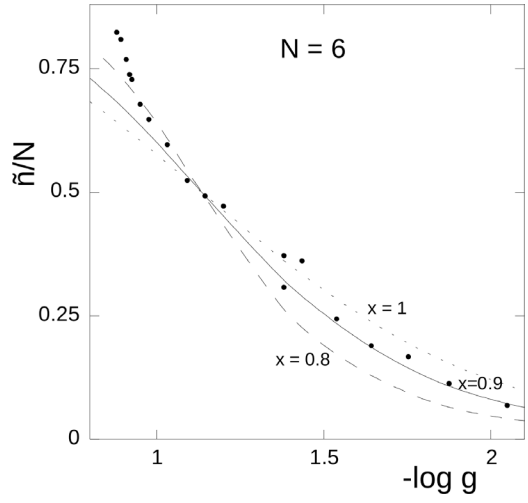

Fig. 10. Degree of complex formation of NA (•) in supercritical CO_2 at 323 K against $-\log g$. The lines are obtained from (19) with $N = 6$ and $x = 0.9$ (solid line), $x = 0.8$ (dashed line), and $x = 1$ (dotted line).

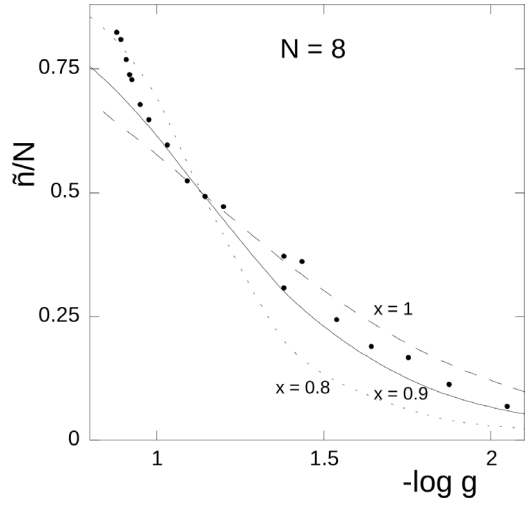

Fig. 11. Degree of complex formation of NA (•) in supercritical CO_2 at 323 K against $-\log g$. The lines are obtained from (19) with $N = 8$ and $x = 0.9$ (solid line), $x = 1$ (dashed line), and $x = 0.8$ (dotted line).

at 323 K against the negative logarithm of g are plotted in Figures 10 and 11 along with the predictions of (19) for values of the parameter $x = 1$ (statistical case), $x = 0.9$, and $x = 0.8$ (the constants are slightly closer in value than predicted statistically while maintaining the overall formation constant β_n equal); in Figure 10 the value of the maximal n or coordination number $N = 6$ and in Figure 11 $N = 8$. In either figure the data below $\tilde{n}/N = 0.5$ are well fitted by values of x

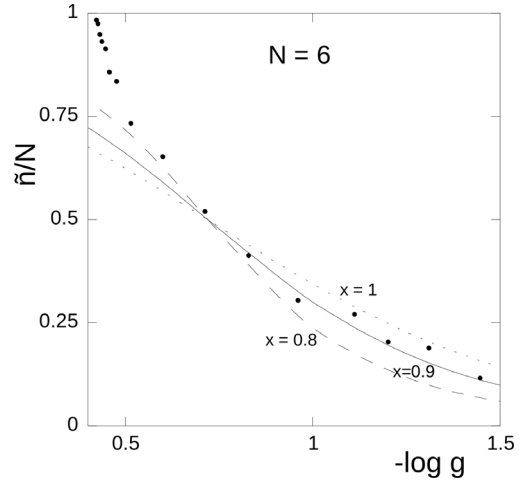

Fig. 12. Degree of complex formation of NA (•) in supercritical CHF_3 at 323 K against $-\log g$. The lines are obtained from (19) with $N = 6$ and $x = 0.9$ (solid line), $x = 0.8$ (dashed line), and $x = 1$ (dotted line).

slightly below 1, however, the data above $\tilde{n}/N = 0.5$ deviate upwards from the prediction somewhat and are not well fitted by any value of x. A similar pattern is observed in Figure 12 for $\tilde{n}/N$ of NA in supercritical CHF_3 at 323 K against pg. Again the values $N = 6$ and $x = 0.9$ fit well the region $\tilde{n}/N < 0.5$ but the deviation in the region above $\tilde{n}/N = 0.5$ is even greater than in the case of the CO_2 data. While it is not surprising that the concentrated solution region presents more difficulty to the fit than the dilute region, thermodynamics alone cannot give clues to the actual mechanism. Without further insight into the molecular interactions taking place the evaluation of the individual constants cannot be pursued further. One possible mechanism in the concentrated region would be the formation of an additional layer of A over the already existing monolayer of A over M.

The number of solute molecules surrounding a solvent molecule as a function of pressure is a difficult question to solve microscopically. Certain assumptions about the solute-solvent interactions (including temperature) must be made before the packing conformations can be ascertained. Numerical [22] and analytical [23] techniques have been pursued on simpler systems as mentioned above. For the similar system (N,N-dimethylamino)benzonitrile in supercritical CHF_3 at 323 K, Kajimoto [18] arrives at a maximum solvation number $N = 7$ based on the radius of the cavity in the Onsager reaction field $a = 0.4$ nm, known or assumed from the calculation of the spectral shift of

the molecule in polar liquids. With a value for the inner surface area of the solvation shell ($4\pi a^2 = 2.0\,\mathrm{nm}^2$) and an estimate of the area occupied by CHF_3 of 0.29 ($= 0.54 \times 0.54$) nm^2 the number $N = 2.0/0.29 \approx 7$ is obtained. The value $N = 8$ for the slightly smaller CO_2 molecule used above appears to agree with this estimate. Further work is clearly needed to elucidate this problem.

7. Conclusions

The theory of Liptay for the effect of the solvent on the wave number of the maximum of the absorption of the solute molecule relative to the gas phase is applicable to supercritical fluids away from the critical point.

Near the critical point of the two supercritical fluids CO_2 and CHF_3 (and of supercritical N_2O from the literature data) the plot of the wave number maximum against the solvent parameter g is broken into three separate regions: a low g or dense vapour region and a high g or high density supercritical fluid region in both of which Liptay's theory is applicable and an intermediate g region which joins the low and the high g regions.

An examination of the location of the intermediate g region in the phase diagram of the two supercritical fluids CO_2 and CHF_3 reveals that this region coincides with the region of the continuous transition from the dense vapour to the supercritical fluid. The intermediate g region where the solvent-solute interactions are altered by small changes in the pressure and the temperature is of practical importance in chromatography, extractions and reaction kinetics; neither the dense vapour region where the solubility is extremely low nor the high density supercritical fluid region where the fluid has the properties of an ordinary solvent are of interest in the applications.

A solvation model based on the theory of complex formation is compatible with the data and serves as an explanation for the appearance of the intermediate region.

Acknowledgements

G. A. A. is grateful for financial assistance from the Akademisches Auslandsamt of the University of Mainz, Germany and the Fondo de Investigaciones de la Facultad de Ciencias de la Universidad de los Andes, Bogotá, Colombia.

[1] J. O. Hirschfelder, C. F. Curtiss, and R. B. Bird, Molecular Theory of Gases and Liquids, John Wiley & Sons, Inc., New York 1967.
[2] J. M. Prausnitz, R. N. Lichtenthaler, and E. Gomes de Azevedo, Molecular Thermodynamics of Fluid-Phase Equilibria, 3rd. ed., Prentice Hall PTR, Upper Saddle River 1999.
[3] W. Liptay, Z. Naturforsch. **20a**, 272, 1441 (1965); **21a**, 1605 (1966).
[4] E. Lippert, Z. Naturforsch. **10a**, 541 (1955).
[5] N. Mataga, Y. Kaifu, and M. Koizumi, Bull. Chem. Soc. Jpn. **29**, 465 (1956).
[6] L. Bilot and A. Kawski, Z. Naturforsch. **17a**, 621 (1962).
[7] N. G. Bakhshiev, Opt. Spectr. USSR **10**, 379 (1961).
[8] W. Baumann, Determination of Dipole Moments in Ground and Excited States, in: Physical Methods of Chemistry: Volume 3B – Determination of Chemical Composition and Molecular Structure, 2nd Ed. (Eds. B. W. Rossiter and J. F. Hamilton), John Wiley & Sons, Inc., New York 1989.
[9] F. Neitzel, Doctoral Dissertation, Mainz, Germany (1999).
[10] G. A. Alvarez, W. Baumann, M. B. Adaime, and F. Neitzel, Z. Naturforsch. **60a**, 641 (2005).
[11] G. A. Alvarez and W. Baumann, Z. Naturforsch. **60a**, 61 (2005).
[12] S. V. Rodrigues, D. Nepomuceno, L. V. Martins, and W. Baumann, Fresenius J. Anal. Chem. **360**, 58 (1998).
[13] T. Moriyoshi, T. Kita, and Y. Uosaki, Ber. Bunsenges. Phys. Chem. **97**, 589 (1993).
[14] T. Makita, H. Kubota, Y. Tanaka, and H. Kashiwagi, Refrigeration **52**, 543 (1977).
[15] A. Kriebel and H. Labhart, Z. Physik. Chemie NF **92**, 247 (1974).
[16] F. Gültekin-Kersch, Dissertation, Mainz, Germany 1989.
[17] C. R. Yonker, S. L. Frye, D. R. Kalkwarf, and R. D. Smith, J. Phys. Chem. **90**, 3022 (1986).
[18] O. Kajimoto, M. Futakami, T. Kobayashi, and K. Yamasaki, J. Phys. Chem. **92**, 1347 (1988).
[19] Y. Kimura and Y. Yoshimura, J. Chem. Phys. **96**, 3085 (1992).
[20] J. K. Rice, E. D. Niemeyer, and F. D. Bright, J. Phys. Chem. **100**, 8499 (1996).
[21] J. Lu, B. Han, and H. Yan, Phys. Chem. Chem. Phys. **1**, 3269 (1999).
[22] I. B. Petsche and P. G. Debenedetti, J. Chem. Phys. **91**, 7075 (1989).
[23] K. Koga, H. Tanaka, and X. C. Zeng, J. Phys. Chem. **100**, 16711 (1996).
[24] I. Prigogine and R. Defay, Chemical Thermodynamics, Longmans Green and Co., London 1954.
[25] J. Bjerrum, Metal ammine formation in aqueous solution: theory of the reversible step reactions, P. Haase and Son, Copenhagen, Denmark 1941.